Received: 30 November 2017 | Revised: 4 February 2018 | Accepted: 7 February 2018

DOI: 10.1002/joc.5501

International Journal of Climatology RMetS

RESEARCH ARTICLE

Climatology and trends of the Euro-Mediterranean thermal bioclimate

Theodore M. Giannaros[1] | Vassiliki Kotroni[1] | Konstantinos Lagouvardos[1] | Andreas Matzarakis[2,3]

[1]National Observatory of Athens, Institute for Environmental Research and Sustainable Development, Athens, Greece

[2]Research Center Human Biometeorology, German Meteorological Service, Freiburg, Germany

[3]Chair of Environmental Meteorology, Faculty of Environment and Natural Resources, Albert-Ludwigs University, Freiburg, Germany

Correspondence
T. M. Giannaros, National Observatory of Athens, Institute for Environmental Research and Sustainable Development, Vas. Pavlou & I. Metaxa, 15236 Penteli, Athens, Greece.
Email: thgian@noa.gr

Funding information
European Commission, Grant/Award Number: 675121

High-resolution numerical simulations were carried out for the most recent 30-year period (1987–2016), focusing on the Euro-Mediterranean region. A sophisticated thermo-physiologically significant thermal index, namely the physiologically equivalent temperature (PET), was computed for assessing the thermal bioclimate of the study area and for investigating the presence of long-term trends, focusing on bioclimatic extremes. Results indicate that the Euro-Mediterranean thermal bioclimate follows a zonal pattern, upon which topography acts to delineate regional maxima and minima. The conducted time series analysis reveals statistically significant trends that are generally more pronounced for cold extremes. In particular, it is found that the number of days with cold (hot) stress has decreased (increased), with the distribution of PET exhibiting warming of both its cold and warm tail. The south–east Mediterranean and the Balkans are found to be the most responsive to bioclimatic changes, showing coherent and statistically significant warming trends. Overall, the results of this study provide a new point of view of the Euro-Mediterranean climate, which could be of usefulness in a wide range of future applications. The detailed spatio-temporal bioclimatic data could be exploited, for instance, to support applications related to tourism and recreation, highlighting regions with favourable or less favourable thermal comfort conditions. Furthermore, the trend data could be employed for quantifying the vulnerability of certain regions to cold and heat stress, in the context of public health applications.

KEYWORDS

climatology, Euro-Mediterranean, high-resolution, physiologically equivalent temperature, thermal bioclimate, trends, WRF

1 | INTRODUCTION

The influence of ambient thermal conditions on the human body has been a prominent and debated topic in the literature for more than 50 years (Büttner, 1938; Fanger, 1970; Jendritzky, 1991; Kerslake, 1972; Parsons, 2003; Sibbons, 1966). Over the last two decades, human biometeorology, the sub-discipline of biometeorology studying the interactions between the atmospheric environment and human beings, has been experiencing resurgence as a result of the increasing concern about the impact of weather and climate on human health and well-being, especially in the context of climate change (McGregor, 2011). Within this context, several researchers (Jendritzky & Tinz, 2009; Junk, Matzarakis, Ferrone, & Krein, 2014; Kovats & Jendritzky, 2006; Laschewski & Jendritzky, 2002; Parsons, 2003) have highlighted that the most significant environmental information that can be provided to support maintenance of human health, performance and well-being, are thermal conditions. This has been dramatically demonstrated during the exceptionally hot summer of 2003 in Europe (Schär & Jendritzky, 2004), when a heat-related death toll of more than 50,000

 © 2018 Royal Meteorological Society

was recorded (Kosatsky, 2005; Muthers, Laschewski, & Matzarakis, 2017; Robine et al., 2008).

The paramount importance of the thermal environment for human health is attributed to the close relationship between the circulatory system and the thermoregulatory mechanism of the human body (Matzarakis & Amelung, 2008; Matzarakis, Muthers, & Koch, 2011). According to the British Occupational Hygiene Society (BOHS, 1996), the latter is responsible for balancing the human heat budget to external thermal conditions and, consequently, determining the body's internal core temperature. Any disruption of this balancing process will result to a net heat gain/loss, generating heat/cold stress. Heat stress takes place "when a person's environment (air temperature, radiant temperature, humidity and air velocity), clothing and activity interact to produce a tendency for body temperature to rise" (Parsons, 2011). On the other hand, "a thermal load on the body under which greater than normal heat losses are anticipated and compensatory thermoregulatory actions are required to maintain the body thermally neutral" (Holmer, 2011) is defined as cold stress. As for thermal comfort, this can be defined as "that condition of mind which expresses satisfaction with the thermal environment" (Fanger, 1972; ISO7730, 2005; Parsons, 2003). Therefore, the term "thermal environment," which is also referred to as the "thermal bioclimate," ingests both the heat exchanges between the human body and the atmospheric environment (thermal stress), and the body's physiological response (thermal strain; Jendritzky & Tinz, 2009; Matzarakis & Amelung, 2008).

Up to nowadays, the thermal influence of the environment on the human body has been most often assessed in terms of a single parameter, primarily air temperature, or a composite thermal index combining two or more standard meteorological variables (e.g., Carder et al., 2005; Diffenbaugh, Pal, Giorgi, & Gao, 2007; Gosling, Lowe, McGregor, Pelling, & Malamud, 2009; Orosa, Costa, Rodríguez-Fernández, & Roshan, 2014; Poupkou, Nastos, Melas, & Zerefos, 2011; Segnalini, Nardone, & Bernabucci, 2011). From a human-biometeorological point of view, however, this is an inappropriate approach since it neglects several important factors (Matzarakis & Amelung, 2008). These factors were first defined by Fanger (1970) and include air temperature, vapour pressure (humidity), air velocity, solar and thermal radiation (environmental parameters), metabolic heat and clothing insulation (personal parameters). In terms of these fundamental parameters, human biometeorology attempts to predict, at best approximation, how a person feels in a given thermal environment (Vanos, Warland, Gillespie, & Kenny, 2010). In this sense, the effects of all thermal components and the complex interactions between physiology, psychology and behaviour (Yao, Li, & Liu, 2009) need to be taken into account, leading to "the necessity of modelling the human heat balance" (Büttner, 1938).

There is currently a wide array of heat budget-based thermal comfort models (Vanos et al., 2010), which satisfy the fundamental condition that for each index value and regardless of the nature of thermal stress, there is a respective and unique outcome in terms of thermal strain (Błażejczyk, Epstein, Jendritzky, Staiger, & Tinz, 2011). These thermal assessment models are founded on some form of the heat balance equation (Błażejczyk, 1994; Brown & Gillespie, 1986; Fanger, 1972; Höppe, 1999; Jendritzky & Nübler, 1981; Parsons, 2003). Thus, they consider the production of internal heat by metabolic activity, required for carrying out physical and mental activities, and the body-atmosphere heat exchanges by conduction (contact), convection (sensible heat), evaporation (latent heat), respiration (sensible and latent heat) and radiation (shortwave and longwave; Jendritzky & Tinz, 2009).

The implementation of comprehensive thermal assessment models eventually allows for "translating" climate and weather data into human bioclimatological information. Geostatistical methods can be then used for spatially depicting bioclimatic data on maps (e.g., Daneshvar, Bagherzadeh, & Tavousi, 2013; Lin & Matzarakis, 2011; Matzarakis, Rutz, & Mayer, 2010; Morillón-Gálvez, Saldana-Flores, & Tejeda-Martinez, 2004; Svensson, Thorsson, & Lindqvist, 2003; Topay, 2013). However, the accuracy of this method depends heavily on the availability and quality of point data (i.e., observations; Zygmuntowski, Matzarakis, Koch, & Rudel, 2005). When no sufficient observations are available, numerical modelling can provide a convenient alternative solution (Giannaros, Melas, & Matzarakis, 2015).

This paper presents a first attempt to produce a human bioclimatic atlas for the Euro-Mediterranean region, based on high-resolution numerical simulations carried out for a 30-year period. The key aim is to provide a detailed mapping of the thermal bioclimate, investigating also the presence of any long-term trends, in particular focusing on extremes. It is thus anticipated that the conducted analysis will contribute to a better understanding on how the complex physiography of the study area regulates the spatial variability of thermal comfort. Furthermore, the study area itself presents high scientific and socio-economic interest, highlighted as one of the most responsive climate-change hot-spots (Giorgi, 2006) and the world's leading tourist destination (United Nations World Tourism Organization (UNWTO), 2009). Therefore, the results of this study could be also exploited for tourism and recreation applications (e.g., Brosy, Zaninovic, & Matzarakis, 2014; De Freitas, Matzarakis, & Scott, 2007; Endler & Matzarakis, 2011), as well as for quantifying the vulnerability of certain regions to cold and heat stress (e.g., Nastos & Matzarakis, 2006, Muthers, Matzarakis, & Koch, 2010). In this wider sense, the present work deviates from past studies that could be considered to be relevant, but focused on deriving future projections without investigating in detail present human

bioclimatic conditions. In addition, they often adopted coarse spatial resolutions (e.g., Jendritzky & Tinz, 2009; Matzarakis & Amelung, 2008), considered a particular type of thermal stress (e.g., Amengual et al., 2014) or even applied a non-thermo-physiological approach (e.g., Diffenbaugh et al., 2007).

2 | MATERIALS AND METHODS

2.1 | Study area

This study focuses on the European Mediterranean (Figure 1a), a region that has been reported to be one of the most responsive climate change hot-spots (Giorgi, 2006). Climatologically, the study area is characterized as highly heterogeneous (Bolle, 2002). The weather patterns and the climate of the Mediterranean are strongly influenced by dry warm air originating from North Africa, dry cold air coming from the Atlantic Ocean, and moist warm air from the Mediterranean Sea itself (Lionello et al., 2006). The physiography of the region itself is also highly complex (Figure 1a), so that fine-scale processes associated with the land/sea contrast, land use heterogeneity and the complicated topography are expected to play a key role in shaping the magnitude and the spatial variability of thermal bioclimatic conditions.

2.2 | Numerical modelling strategy

Numerical simulations were conducted with the Weather Research and Forecasting (WRF) model, version 3.7.1 (Skamarock et al., 2008). The model was configured with the Lin microphysics parameterization (Lin, Farley, & Orville, 1983) and the RRTMG (Rapid Radiative Transfer Model) scheme for parameterizing shortwave and longwave radiation (Iacono et al., 2008). The Yonsei University (YSU) scheme (Hong, Noh, & Dudhia, 2006) was chosen for representing planetary boundary-layer processes, coupled with the MM5 similarity surface-layer parameterization (Zhang & Anthes, 1982). Land-surface processes were handled with the Unified Noah land-surface model (Tewari et al., 2004), while convection was parameterized with the Grell three-dimensional (3D) ensemble scheme (Grell & Devenyi, 2002).

A single domain with a horizontal grid spacing of 0.11° × 0.11° (~12 × 12 km^2) and a mesh size of 738 × 497 grid points was defined for carrying out the simulations (Figure 1b). The modelling domain extends from 2° to

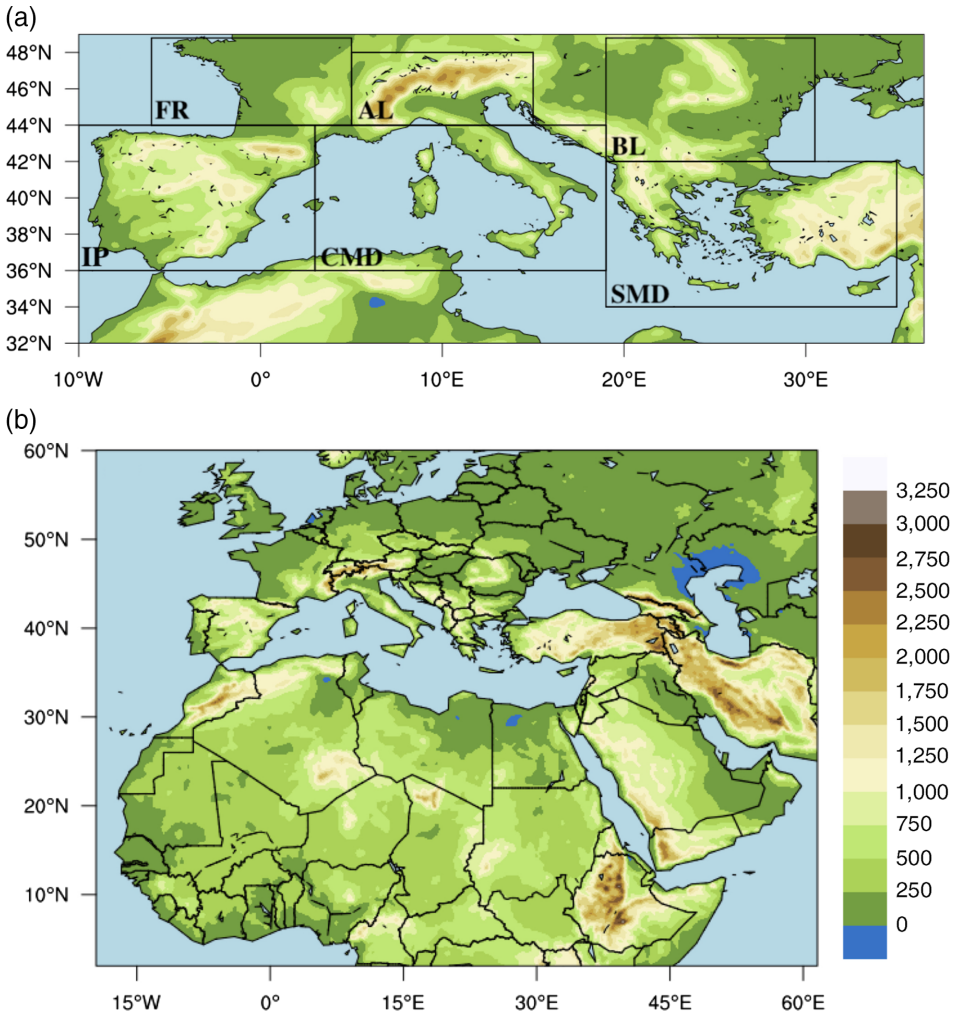

FIGURE 1 (a) Zoom over the study area with identification of the analysis regions [IP: Iberian Peninsula (−10°–3°E, 36°–44°N), FR: France (−6°–5°E, 44°–49°N), AL: Alps (5°–15°E, 44°–48°N), CMD: Central Mediterranean (3°–19°E, 36°–44°N), BL: Balkans (19°–30.5°E, 42°–49°N), SMD: south–east Mediterranean (19°–35°E, 34°–42°N)]. (b) Model-resolved topography in the numerical simulation domain. The colour scale is common to both maps [Colour figure can be viewed at wileyonlinelibrary.com]

TABLE 1 Ranges of PET for different grades of human thermal perception and thermo-physiological stress (Source: Matzarakis & Mayer, 1997)

PET (°C)	Thermal perception	Thermo-physiological response
< 4	Very cold	Extreme cold stress
4–8	Cold	Strong cold stress
8–13	Cool	Moderate cold stress
13–18	Slightly cool	Slight cold stress
18–23	Comfortable	No thermal stress
23–29	Slightly warm	Slight heat stress
29–35	Warm	Moderate heat stress
35–41	Hot	Strong heat stress
>41	Very hot	Extreme heat stress

60°N, and from 20°W to 62°E. In the vertical, 35 unequally spaced full sigma levels were defined, with the model top set at 50 hPa. The 0.75° × 0.75° spatial resolution and 6 hr temporal resolution ERA-Interim global reanalysis dataset (Dee et al., 2011) was employed for driving the WRF simulations. The model was implemented for the 30-year period extending from January 1, 1987 to December 31, 2016. The numerical simulations were conducted by reinitializing WRF every 10 days with the ERA-Interim reanalysis data and including an overlap period of 12 hr for each simulation block for spinning up meteorology. Sea-surface temperature was updated at 6 hr intervals and no nudging was applied.

2.3 | Thermal assessment strategy

The physiologically equivalent temperature (PET) thermal assessment scheme (Höppe, 1999) was used for evaluating the thermal bioclimate of the study area. This scheme is based on the Munich Energy Balance Model for Individuals (MEMI), which simulates the thermal condition of the human body in a thermo-physiologically significant way (Höppe, 1993). PET can be defined as the air temperature at which, in a typical indoor environment with the absence of wind and solar radiation, the heat budget of the human body is balanced with the same skin and internal core temperature as under the influence of the complex outdoor conditions that are assessed. Following Höppe (1999) and Matzarakis, Mayer, and Iziomon (1999), the effect of air temperature on PET is taken into account through the convective heat flow and the heat flows used for heating and humidifying the air that is respired. The water vapour influence is restricted to the exchange of latent heat through diffusion and respiration via the skin, whereas latent heat fluxes originating from the evaporation of sweat are not considered. The effect of wind is accounted for through the heat loss by evaporation and convection. The mean radiant temperature (TMRT) of the surroundings is used for considering the net radiation of the human body, while thermo-physiology is taken into account by means of human activity (added to a reference metabolic heat production rate) and clothing insulation.

PET is a comfort-based thermal index that, apart from being thermo-physiologically relevant, has the advantage of a widely known unit (i.e., °C). This facilitates its interpretation and communication to people and stakeholders that are not familiar with the terminology of human biometeorology. The assessment scale of PET (Table 1) is derived by computing the predicted mean vote (PMV; Fanger, 1972) for different air temperatures in the reference environment, using the reference person's setting (Matzarakis & Mayer, 1997). This assessment scale classifies PET values according to human thermal perception and thermo-physiological response, in compliance with the standard nine-point ASHRAE (American Society for Heating Refrigerating and Air-Conditioning Engineers) thermal sensation scale.

TABLE 2 Definitions of the 10 PET-based indices used for evaluating thermal bioclimate extremes. Unless explicitly indicated, indices are computed using both 0000 UTC and 1200 UTC PET values, representing night-time and daytime conditions, respectively

Index	Description	Definition	Units
PET8	Cold nights	Annual count of days with PET<8 °C at 0000 UTC	Days
PET4	Very cold nights	Annual count of days with PET<4 °C at 0000 UTC	Days
PET35	Hot days	Annual count of days with PET>35 °C at 1200 UTC	Days
PET41	Very hot days	Annual count of days with PET>41 °C at 1200 UTC	Days
PETn	Coldest day/night	Monthly minimum value of PET	°C
PETx	Hottest day/night	Monthly maximum value of PET	°C
PETp95	Extremely hot PET	Annual 95th percentile PET	°C
PETp75	Very hot PET	Annual 75th percentile PET	°C
PETp5	Extremely cold PET	Annual 5th percentile PET	°C
PETp25	Very cold PET	Annual 25th percentile PET	°C

2.3.1 | Computation of PET

The RayMan Pro model (Matzarakis, Rutz, & Mayer, 2007, 2010), version 2.3, was employed for calculating PET. RayMan is a radiation and human bioclimate micro-scale model, which allows for deriving thermal assessment indices, including PET, on the basis of computing TMRT and solving the human heat balance equation. The WRF simulations (section 2.2) were employed for deriving the forcing data for RayMan, that is 2-m air temperature and relative humidity, wind speed (interpolated to 1.1 m, which approximates the weighting height of the human body, following Charalampopoulos, Tsiros, Chronopoulou-Sereli, & Matzarakis, 2013), global radiation and surface temperature. Due to computational restrictions, the model was implemented only for the WRF's land grid points between 32° and 49°N, and 10°W and 36.5°E (Figure 1a). PET was consequently

computed for 0000 UTC and 1200 UTC in order to derive, at best approximation, the minimum and maximum thermal perception of each day (Amengual et al., 2014). The human biometeorological assessment of thermal perception, expressed via PET, was conducted, after Matzarakis et al. (1999), for a standard 35-year-old male, 1.75-m tall, weighting 75 kg, wearing clothes with an insulation of 0.90 clo (1 clo corresponds to heat resistance of 0.155 K W^{-1}) and having a metabolic heat production rate of 80 W (light activity).

2.4 | Bioclimate extremes

The analysis of the Euro-Mediterranean thermal bioclimate was conducted using a set of 10 PET-based indices, defined at 0000 UTC and/or 1200 UTC (Table 2). These indices were specified so as to represent absolute bioclimate extremes (PETn, PETx), threshold-dependent extremes (PET8, PET4, PET35, PET41) and percentile-based extremes (PETp95, PETp75, PETp5, PETp25). All calculations were carried out with the ICCLIM (Indice Calculation CLIMate) python library, version 4.2.9 (https://github.com/cerfacs-globc/icclim) and/or the Climate Data Operators (https://code.mpimet.mpg.de/projects/cdo/), version 1.7.0.

Maps of the spatial pattern of the indices, averaged over the 1987–2016 period, were constructed for compiling the recent climatology of Euro-Mediterranean thermal bioclimate. For evaluating the presence of long-term trends, the nonparametric Mann–Kendall (MK) test (Kendall, 1976; Mann, 1945) was employed. The pre-whitening test of Yue-Pilon (Yue, Pilon, Phinney, & Cavadias, 2002) was applied prior to the implementation of the MK test in order avoid the effect of any positive serial correlation in the examined datasets. For this purpose, the ZYP package of R (https://cran.r-project.org/web/packages/zyp/index.html) was used.

2.5 | Observations and evaluation procedure

Recent studies have shown that the fluctuations of air temperature are the key determinant of PET's variations (Basarin et al., 2017; Chen & Matzarakis, 2017; Giannaros et al., 2015). Considering this, prior to the assessment of the thermal bioclimate of the study area, the performance of the WRF model was evaluated focusing on air temperature. The E-OBS version 15.0 (hereafter referred to as EOBS15) daily minimum (TN) and maximum (TX) temperature data (Haylock et al., 2008), available on a regular 0.25° x 0.25° grid, were employed for assessing the spatial variability of model bias. Taking into account the difficulty in interpreting the whole annual bias, which stems from the different model behaviour depending on the season (Garciá-Diéz, Fernández, Fita, & Yagüe, 2013), the analysis was carried out on a seasonal basis, focusing on winter (DJF) and summer (JJA). In addition and to draw the wider picture, a comparison of mean annual cycles, spatially averaged over six different regions (Figure 1a), was conducted. It should be noted that despite the recently reported inaccuracies in the E-OBS dataset (Hofstra, Haylock, New, & Jones, 2009; Kysely & Plavcova, 2010), the relevant mean climatologies are considered to be of reasonable quality (Herrera, Fita, Fernández, & Gutiérrez, 2010) and the presented work will only use these.

To allow for comparisons, the WRF data were bilinearly interpolated to the EOBS15 grid. The model bias was then computed by subtracting the observed from the simulated gridded data. The statistical significance of the differences was verified with a two-independent sample t test (Katragkou et al., 2015). The carried out model evaluation aims at providing basic evidence with respect to the accuracy of the model and the associated uncertainties, which need to be taken into account for the assessment of the thermal bioclimate and the investigation of its long-term trends during the examined time period.

3 | RESULTS

3.1 | Model evaluation

Figure 2 shows the DJF and JJA TX and TN bias of the WRF model, averaged over the 1987–2016 period. A first look reveals that although the model in general underestimates temperatures, differences exist between the examined seasons and variables. In winter, the simulated TX is found to differ significantly (at the 95% confidence level) from the observations over the largest part of the study area, showing biases of approximately −2 °C on average (Figure 2a). TN shows generalized non-significant cold biases over most of the domain, while statistically significant warm biases of up to 2 °C are found mainly over the Iberian Peninsula (IP; Figure 2b). For both TX and TN, the largest negative biases, reaching −6 °C in the case of TN, are found primarily over the Alpine ridge and over regions characterized by steep orography. This is a feature that is rather common to WRF simulations (e.g., Katragkou et al., 2015; Kioutsioukis et al., 2016; Kotlarski et al., 2014), attributed, at least partially, to the treatment of physics over snow-covered areas.

Summertime TX shows widespread statistically significant cold biases that reach −3 °C in regions with good EOBS15 data quality (e.g., Spain; Figure 2c). Larger negative biases, exceeding −5 °C, are found for several grid points across the domain, mainly over the Balkans (BL) and the northern regions of Turkey. On the other hand, the model is found to be less biased cold for TN, with generalized non-significant negative biases dominating the largest part of the Euro-Mediterranean region (Figure 2d). Statistically significant warm biases of up to 2–3 °C are mainly found over the eastern part of the domain. The large area of warm bias emerging over North Africa, evident in both TX and TN, has been also reported in previous modelling

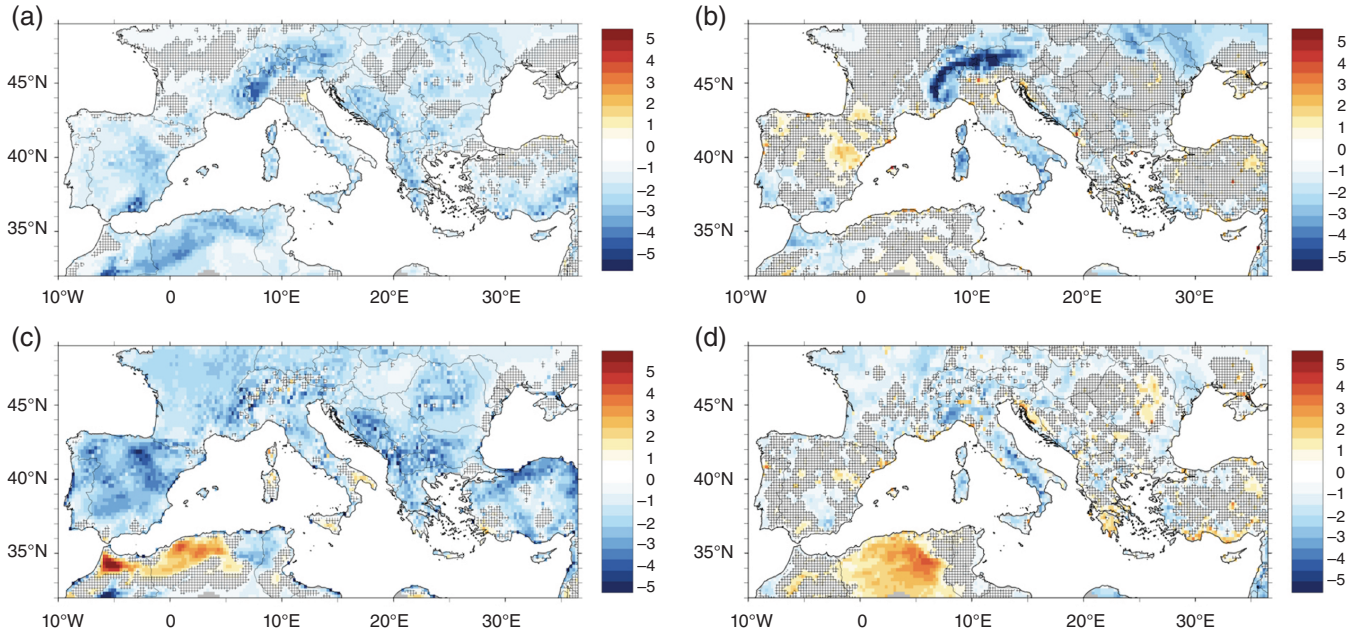

FIGURE 2 Daily maximum (a, c) and minimum (b, d) temperature bias (WRF–EOBS15), averaged over the 1987–2016 winter (top row) and summer (bottom row). Units are in °C. Hatching indicates grid points where the biases are not statistically significant ($\alpha = .05$) [Colour figure can be viewed at wileyonlinelibrary.com]

studies (Garciá-Diéz, Fernández, & Vautard, 2015; Katragkou et al., 2015; Kioutsioukis et al., 2016) and is most probably attributed to the excessive interpolation of scarce EOBS data (Garciá-Diéz et al., 2013).

The presented maps in Figure 2 indicate the existence of a seasonal dependence of model bias, with differences also existing between maximum and minimum temperatures. Hence, it can be assumed that different biases exist in different parts of the temperature range. To verify this, the methodology of Garciá-Diéz et al. (2013), based on the construction of quantile–quantile (q-q) plots, was employed. In this context, the distributions of the simulated TX and TN (y-axis) were compared against observations (x-axis), by dividing the entire probability range into 19 pieces (i.e., considering a quantile every 5%). This kind of representation allows for highlighting deviations in the probability distribution (denoted as departures from a straight diagonal line), biases (denoted as shifts), variability differences (denoted as straight lines with different slopes) and asymmetries (denoted as curved lines). Q-q plots were constructed for the six specified regions of the European Mediterranean (Figure 1a), for both TX and TN. No averaging was carried out for computing the quantiles.

As shown in Figure 3, the model behaviour differs depending on both the region considered and the temperature. DJF and JJA TX (Figure 3a) present systematic cold biases over the warmest of the examined regions, namely IP, Central Mediterranean (CMD) and south–east Mediterranean (SMD). Over these regions and for both seasons, the simulated and observed TX follow the same probability distribution, as highlighted by the alignment of the points along an approximately straight line, with all the WRF-derived quantiles shifted 1–2 °C to cooler temperatures. The distributions of observed and modelled TX are found to differ over the remaining three regions, with the coolest Alps (AL) and BL showing similarities in terms of model behaviour. In particular, asymmetries are evident in the simulated DJF TX, since the points in the q-q plots appear to follow slightly curved lines, with the largest biases (up to −3 °C for AL and −2 °C for BL) found for the lowest quantiles (temperatures below 0 °C).

Focusing on minimum temperatures (Figure 3b), the model shows a rather consistent behaviour. In almost all regions, the modelled and observed wintertime distributions of TN differ more on the lower quantiles. This is most pronounced in the AL and BL regions, in which biases reach up to −6 and −3 °C on the lowest 5% quantiles, respectively. This reflects what has been earlier noted to be a common feature of WRF simulations in cold and often snow-covered areas. In the rest of the regions, the differences between the model and the observations do not exceed 1–2 °C, with lowest values found on the upper quantiles. In summer and in five of the six regions, the points in the q-q plots are aligned along straight lines that deviate from the diagonals, suggesting differences between the probability distributions of observed and simulated TN. In particular, the lower quantiles of TN are found to be biased cold in all regions. This bias appears to disappear in upper quantiles, while in the warmer IP and SMD regions; it even turns to positive values (overestimation) when TN exceeds 19–20 °C. Under all cases, the JJA observed and model-derived quantiles show differences that do not exceed 2 °C.

The results of the gridded verification and the q-q analysis focusing on DJF and JJA provide evidence for a

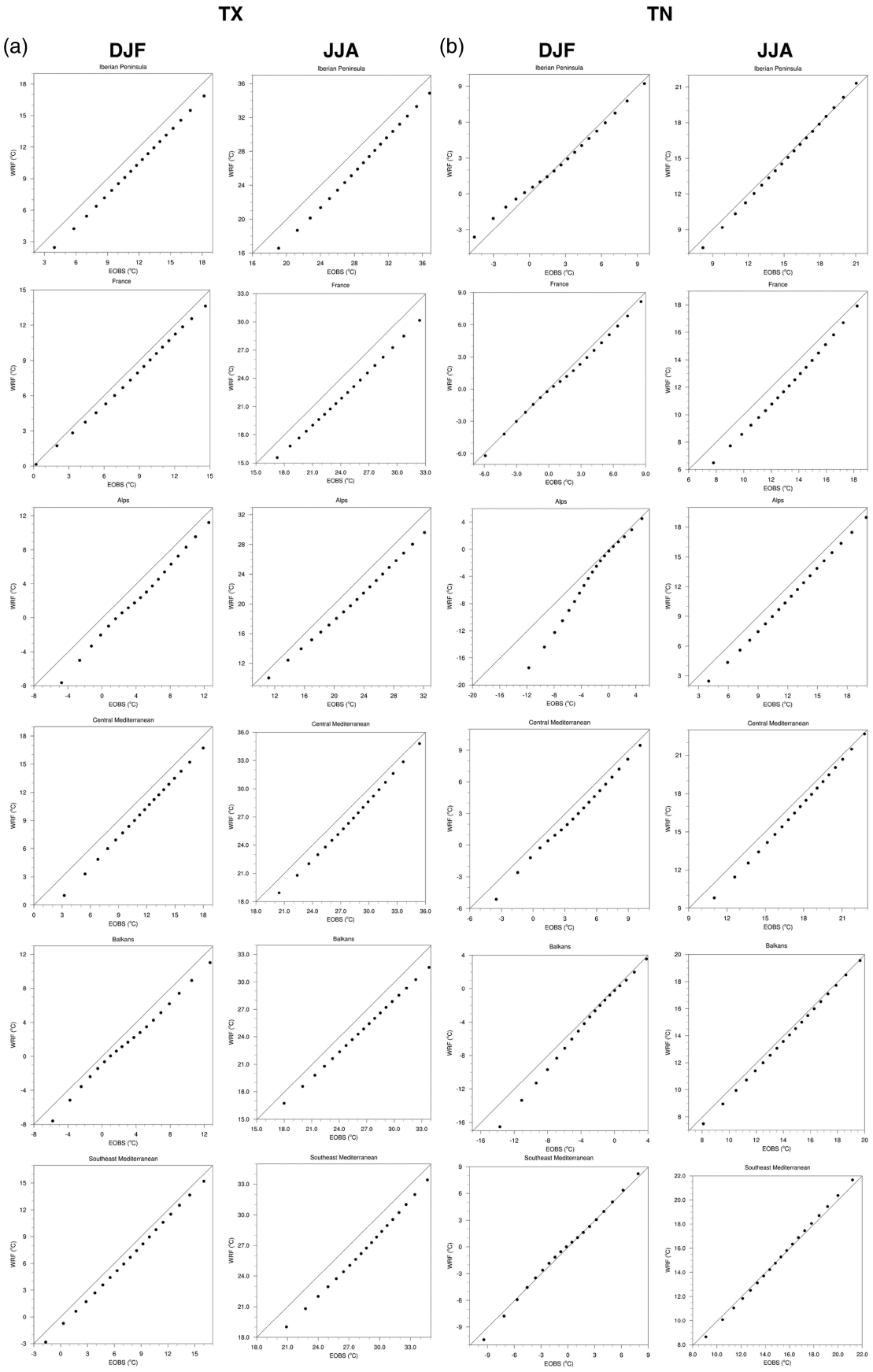

FIGURE 3 Quantile–quantile plots for the daily (a) maximum and (b) minimum temperature, and for the six regions (rows) of the study area. Mind the differences in the axes' scales

reasonable overall model performance. In addition, the presented maps indicate that spatial autocorrelation is generally large enough to allow for deriving meaningful spatial averages. Hence, mean monthly annual cycles were constructed for each of the specified regions of the European Mediterranean (Figure 1a) to get a more detailed perspective of the temporal evolution of model performance.

As shown in Figure 4, the model reproduces successfully the basic characteristics of the mean annual cycles of both temperatures in all regions. The annual cycles are found to be generally biased cold, particularly with respect to maximum temperatures. For the latter, biases are generally larger in summer and winter, though they do not exceed 2 °C in magnitude. In spring and autumn, the modelled mean monthly TX is found to be within 1 °C from observations. Considering TN, biases are found to reach up to −1 °C, mostly pronounced in winter and early spring.

3.2 | Overview of bioclimatic conditions

Thermal bioclimate diagrams (Matzarakis, 2007; Zaninovic & Matzarakis, 2009) were constructed for each of the examined regions (Figure 5) in order to draw the general picture of the prevailing bioclimatic conditions. These diagrams present the frequencies of the simulated 0000 UTC and 1200 UTC PET values, computed over 10-day intervals for the 1987–2016 period.

In the night-time (Figure 5a) and in all regions, neutral and near-neutral thermal conditions (13 °C < PET<29 °C) occur from late spring to early summer [third (first) 10-day period of May (June)] until early to mid-autumn [first (second) 10-day period of September (October)]. Not surprisingly, the warm IP, CMD and SMD regions show the largest frequencies of such conditions, reaching up to 50–60% in July and August. These regions also exhibit a shorter period of prevailing (>50%) strong cold stress conditions (PET < 8 °C; October to May) compared with the colder France (FR), AL and BL (September to June/July). As for extreme cold stress (PET<4 °C), it is found to occur most often from mid-October to early November until early to mid-May in IP, FR, CMD and SMD, and from mid-September to early October until May in AL and BL. January and February, showing the lowest mean

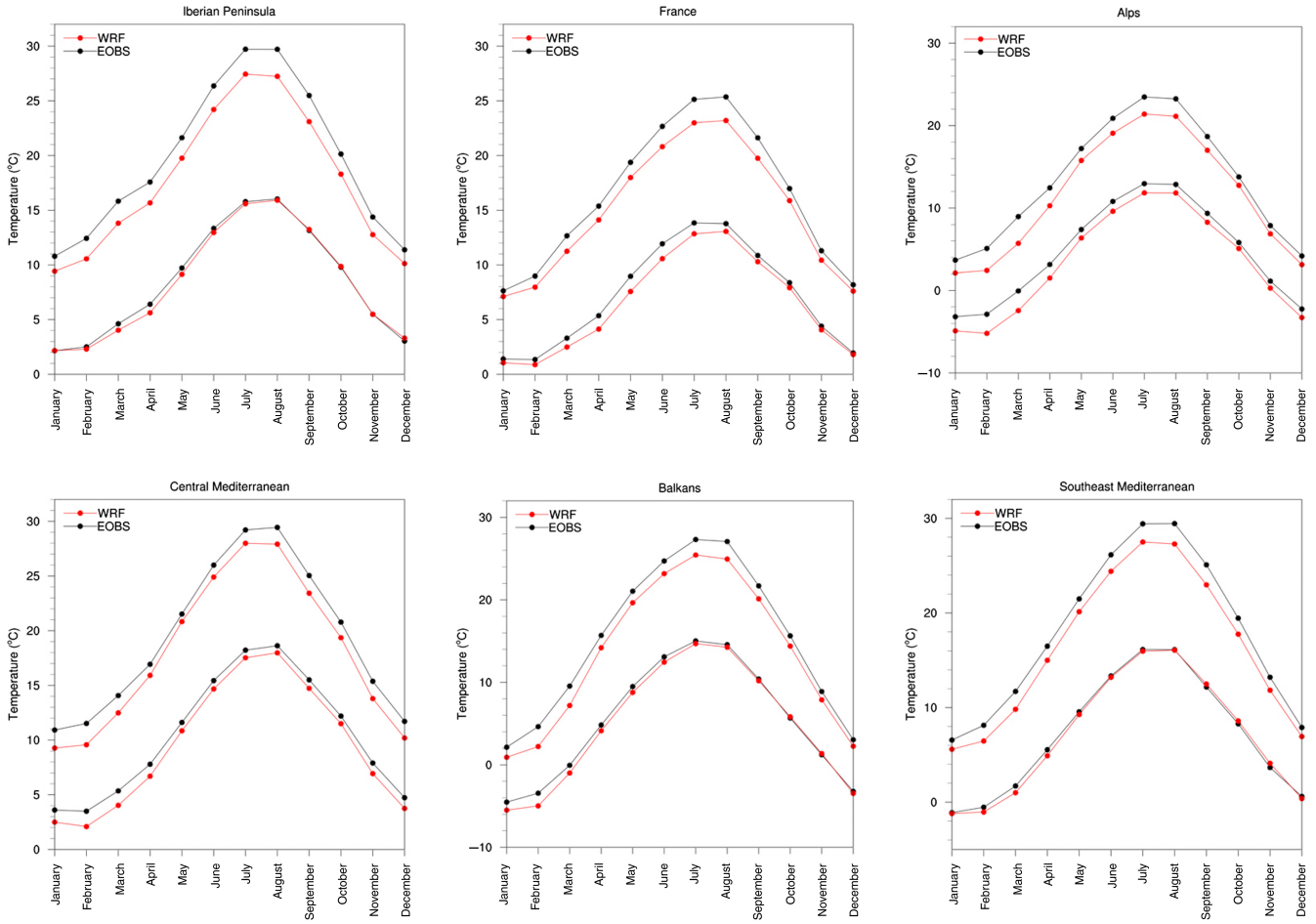

FIGURE 4 Mean annual cycles of daily maximum and minimum temperatures, spatially averaged over the six regions of the study area. The upper (lower) pair of curves in each plot corresponds to the maximum (minimum) temperature. Mind the differences in the y-axis scales [Colour figure can be viewed at wileyonlinelibrary.com]

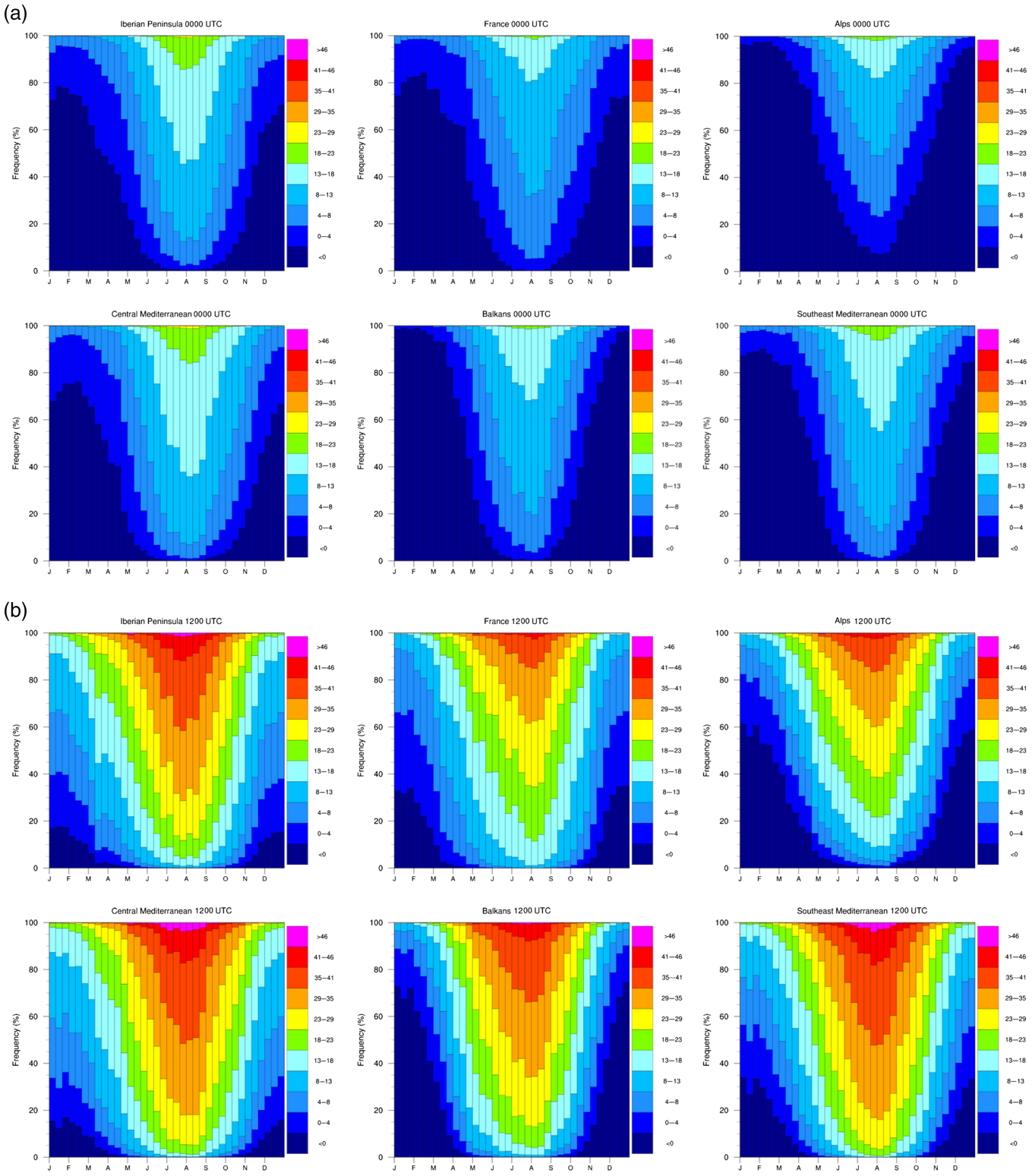

FIGURE 5 Model-based (a) night-time (0000 UTC) and (b) daytime (1200 UTC) thermal bioclimate diagrams for the six examined regions, for the 1987–2016 period. Units are in °C [Colour figure can be viewed at wileyonlinelibrary.com]

monthly minimum temperatures (Figure 4), are the months with the highest frequencies of negative PET.

Heat stress conditions (PET > 29 °C) are found in daytime and in all regions examined (Figure 5b). As expected, such conditions prevail in the warm IP, CMD and SMD, but also in BL, for a period of approximately 2 months, starting mid/end of June and spanning through August. Heat stress is also found occurring in the cooler FR and AL, with highest frequencies (up to ~40%) from mid-July to mid-August. Considering extreme heat stress (PET > 41 °C), it occurs in all regions but with clearly higher frequencies, reaching up to 15–20% in July and August, in IP, CMD and SMD. Daytime strong cold stress conditions (PET < 8 °C) occur most often during winter and autumn in FR, AL and

BL, and during winter in IP, CMD and SMD. In the latter regions, extreme cold stress (PET < 4 °C) occurs primarily in winter but with frequencies that do not generally exceed 50%. In contrast, FR, AL and BL exhibit such conditions more frequently, for up to 60–90% of days in December and January. Finally, neutral and near-neutral thermal conditions (13 °C < PET<29 °C) show frequencies greater than 15–20% all year round in the warmest regions (IP, CMD, SMD), whereas in the FR, AL and BL they are typically found from March to mid-November. In all regions, these conditions occur more often in spring and autumn.

3.3 | Cold extremes (PET8, PET4, PETn, PETp5, PETp25)

3.3.1 | Climatology

Figure 6 summarizes the model-derived 1987–2016 climatologies of cold bioclimate extremes indices in the Euro-Mediterranean region. Cold (PET8) and very cold (PET4) nights show a south–north gradient that is characteristically shaped by topography (Figure 6a,b). The southern coastal areas of the IP, FR, Italy, Greece, Turkey and Cyprus are found to experience approximately 200–250 cold nights, of which about 80–160 days can be characterized as very cold. With increasing latitude and altitude, the number of nights with cold and very cold thermal perception increases and reaches up to more than 300 and 250 days, respectively, with the highest values found over the most elevated regions. It is also worth noticing that major urban areas (e.g., Paris, Muenchen, Wien, Budapest, etc.) can be identified in the spatial pattern of both PET8 and PET4 as grid points with considerably lower values compared with their surroundings. This is clearly the result of the nocturnal urban heat island effect, which mitigates cold stress by maintaining elevated temperatures within the urban areas compared with their rural surroundings (Giannaros & Melas, 2012).

Considering the absolute intensity of cold stress, represented by PETn (Figure 6c,d), it appears that it follows the spatial variability of the daily minimum temperature (Figure 4). The lowest mean annual PETn values are found over the cold AL and the BL, reaching up to −35 and −25 °C in night-time (0000 UTC) and daytime (1200 UTC), respectively. Significantly higher values, up to −5 °C (2 °C) at 0000 UTC (1200 UTC), are simulated for most of the warmer IP and the southernmost parts of central and south-east Euro-Mediterranean region. Overall, the 1987–2016 climatology of PETn shows a west–east gradient, with the coldest nights and days found over the eastern and more continental parts of the study area. It is also evident that the coldest nights exhibit negative PET values (i.e., extreme cold stress) throughout the domain (Figure 6c), whereas positive values (i.e., moderate cold stress) may be found along the southern coastal areas during the day (Figure 6d).

Examination of the mean annual spatial pattern of PETp5 (Figure 6e,f) and PETp25 (Figure 6g,h) reveals again the key influence of topography on determining the spatial variations of the cold tail of PET's distribution. Major orographic features of the Euro-Mediterranean region, such as the Pyrenees, the Alps, the Dinaric Alps and the Carpathians, can be clearly distinguished as regions of domain-wide minimum percentile values, with the southern parts of the domain showing much milder PETp5 and PET25 values. Further inspection of Figure 6e–h indicates that the lowest night-time 5th and 25th percentile PETs do not exceed 5 °C throughout the entire study area, thus corresponding to strong cold stress conditions. In the presence of solar radiation, the cold tail of the distribution of daytime PET shifts towards warmer values, reaching up to neutral and near-neutral comfort conditions.

3.3.2 | Trends

Figure 7 presents the 30-year long-term trends of cold bioclimate extremes, derived from the analysis of the WRF simulations. At a first glance, it is evident that the model suggests a decrease in the number of cold (PET8) and very cold (PET4) nights (Figure 7a,b). For both PET8 and PET4, statistically significant ($p < .10$) negative trends are found over almost the entire European Mediterranean. The decreasing trends, reaching values of up to 1.5 days year^{-1}, are widespread and most pronounced over the south–east parts of the Euro-Mediterranean region, including the BL. Non-significant positive trends (0.5 days year^{-1}) exist over parts of the IP, FR and the AL.

Contrary to the threshold-dependent PET8 and PET4 indices, the absolute extreme PETn index shows no preferential change during the examined 30-year period (Figure 7c,d). Considering both day and night, almost equally distributed, non-significant increasing and decreasing trends of up to ±0.3 °C year^{-1} characterize the presented maps. Statistically significant trends are found to be primarily of negative sign, indicating intensification of cold stress conditions during the coldest days and nights. However, these trends appear not to follow any particular spatial pattern. Instead, they are sparsely distributed mainly over the eastern BL, along the Black sea coastline, the IP and FR.

Examination of the 1987–2016 trends per year of percentile PETs reveals a cooling/warming dipole, seen both in night-time (Figure 6e,g) and daytime (Figure 6f,h). As shown, the Euro-Mediterranean region can be divided into two parts, each dominated by trends of opposite sign. In general, the west part is characterized by non-significant negative trends that do not exceed −0.1 °C year^{-1} for both PETp5 and PETp25. Some statistically significant trends are mainly found for daytime PETp25 over the IP, suggesting cooling (<0.1 °C year^{-1}) of the cold tail of PET's distribution (Figure 6f). Widespread positive trends are found over the eastern part of the domain. For the cold extremes of the

PET distribution, represented by PETp5, the positive trends show no statistical significance except over small parts of Greece and Turkey (Figure 6e,f). On the other hand, there is a clear and statistically significant warming trend for night-time PETp25 (Figure 6g), which reaches up to 0.15 °C year^{-1} in the northern and eastern parts of the Balkan Peninsula. This trend is also evident for daytime PETp25 but with statistical significance restricted over the southernmost parts of south–east European Mediterranean (Figure 6h).

Trends with different levels of statistical significance for the previously discussed indices are summarized in Table 3. The presented trends per decade were computed using spatial averages of the indices over the specified regions of the study area (Figure 1a). Results indicate that cold (PET8) and very cold (PET4) nights have been decreasing substantially throughout the study area over the course of the 1987–2016 period. The largest, statistically significant ($p \leq .01$) trends are found for BL and SMD, approximating −6 to −7 days per decade. Cold stress conditions during the coldest night and day (PETn) show both increasing and decreasing trends that are non-significant in all regions except for the IP, for which the reported trend suggests a

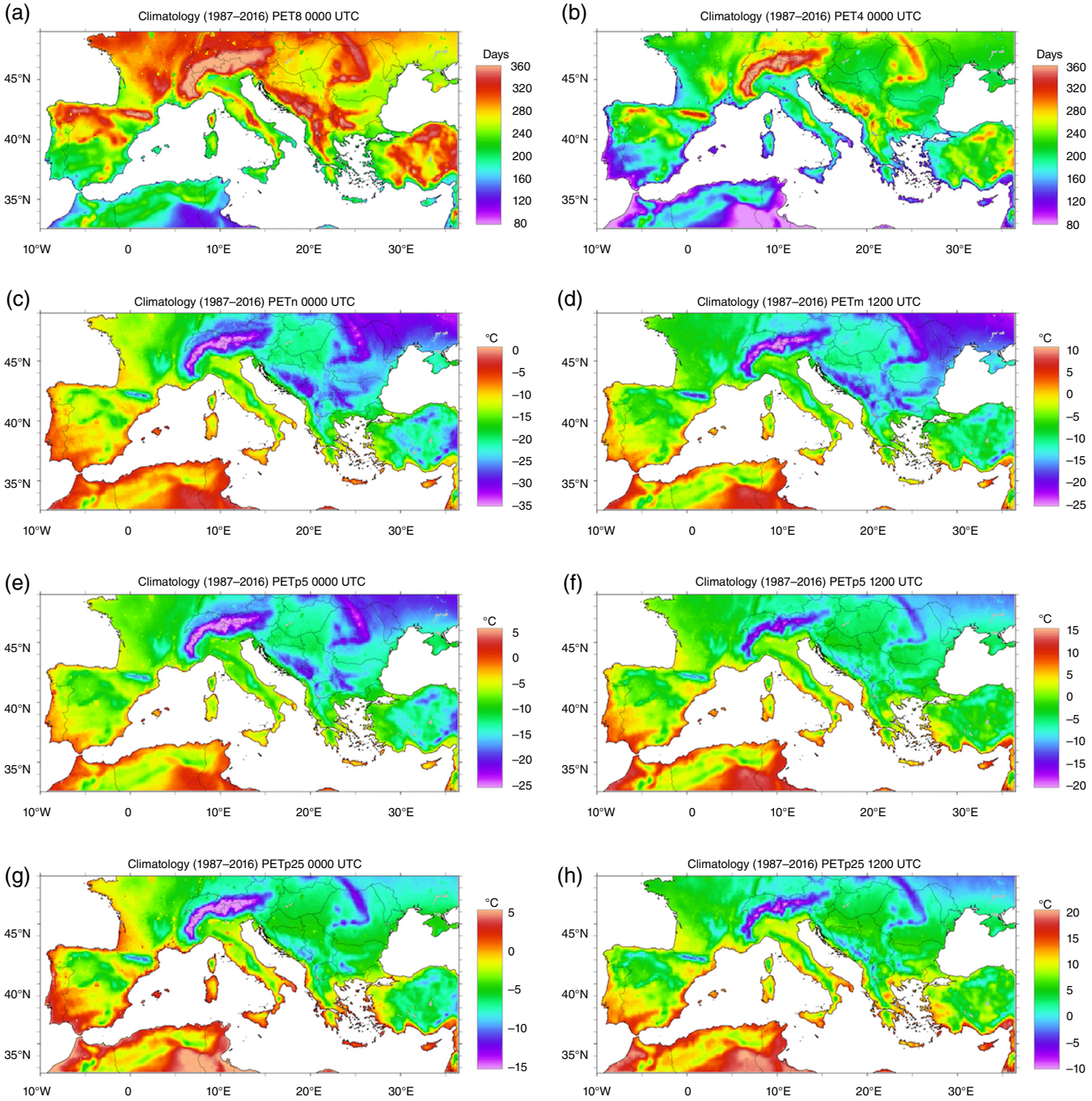

FIGURE 6 The 1987–2016 time mean of (a) PET8, (b) PET4, (c) 0000 UTC PETn, (d) 1200 UTC PETn, (e) 0000 UTC PETp5, (f) 1200 UTC PETp5, (g) 0000 UTC PETp25 and (h) 1200 UTC PETp25. Mind the differences in the scales [Colour figure can be viewed at wileyonlinelibrary.com]

statistically significant ($.05 < p \leq .10$) decrease of nighttime PETn. The IP is also found to be the only region with a statistically significant ($.01 < p \leq .05$) cooling trend of −0.21 °C per decade for PETp5, whereas positive, but non-significant, warming trends are found for the rest of the Euro-Mediterranean region. Last, statistically significant warming trends are found for PETp25 for the eastern part of the domain (BL, CMD, SMD), with the largest values (0.5–0.6 °C per decade) computed for SMD. All in all, the results shown in Table 3 provide evidence for a warming of the cold facet of the thermal bioclimate, most pronounced over south–east European Mediterranean.

3.4 | Hot extremes (PET35, PET41, PETx, PETp75, PETp95)

3.4.1 | Climatology

The model-based 1987–2016 climatologies of hot bioclimate extremes indices in the Euro-Mediterranean region are presented in Figure 8. Lowland areas can be clearly seen as hot-spots with the most hot (PET35) and very hot days (PET41) across the entire domain (Figure 8a,b). This is particularly true for the Andalusian Plain in south–west Spain, the Thessaly Plain and the Axios Valley in central and northern Greece, respectively, and the western plains of Turkey bordering with the Aegean Sea, for which 90 hot

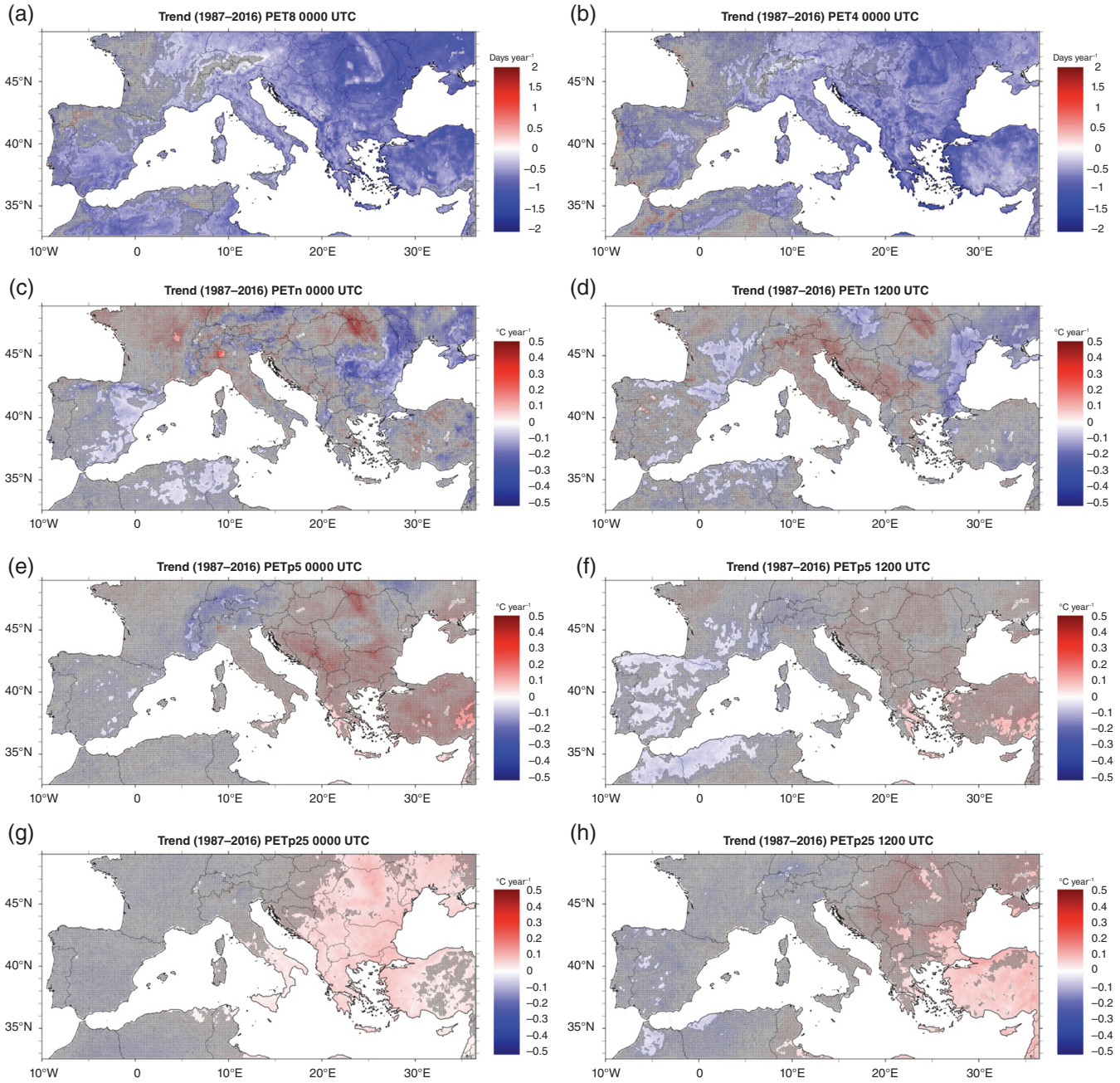

FIGURE 7 The 1987–2016 trend per year of (a) PET8, (b) PET4, (c) 0000 UTC PETn, (d) 1200 UTC PETn, (e) 0000 UTC PETp5, (f) 1200 UTC PETp5, (g) 0000 UTC PETp25 and (h) 1200 UTC PETp25. Hatching indicates grid points where the trends are not statistically significant, at least at the 90% confidence level ($p > .10$). Mind the differences in the scales [Colour figure can be viewed at wileyonlinelibrary.com]

and 40–50 very hot days per year can be considered as typical. PET35 and PET41 decrease with increasing altitude and latitude, reaching values close or equal to zero for the most elevated areas.

The night-time mean annual monthly maximum PET (PETx) shows a fairly smooth and, more or less, homogeneous spatial pattern, with specific features superimposed on it. As shown in Figure 8c, values between 15 and 20 °C are widespread across the entire study area, except from the lowlands of south–west Spain where PETx is found to exceed 23 °C (i.e., slight heat stress). On top of this background, high-altitude regions are delineated by lower values that correspond to moderate and strong cold stress conditions (4 °C < PET<13 °C). Major urban areas (e.g., Porto, Madrid, Paris, Milan, Budapest, Belgrade, etc.) can be also recognized by the higher PETx values compared to their surroundings, as a result of the nocturnal urban heat island effect (Giannaros & Melas, 2012). On the other hand, although it is influenced by topography, the daytime spatial distribution of PETx shows a more zonal pattern (Figure 8d). The highest values, reaching up to more than 50 °C, are found over lowland areas, approximately below the 42°N parallel, decreasing further north and showing local minima over the most elevated areas.

For the largest part of the European Mediterranean, values within the range 10–15 °C, corresponding to slight and moderate cold stress, can be taken as typical for the highest 95th percentile PET during the night (Figure 8e). Higher values, corresponding to thermal comfort (18 °C < PET<23 °C), are found over south–west Spain and over major urban areas. During the day, the spatial pattern of PETp95 shows local maxima up to more than 40 °C (i.e., extreme heat stress) over the lowland continental areas of the Euro-Mediterranean region (Figure 8f). From a health point of view, this is very relevant since these areas are densely populated. Last, similar findings can be reported by inspecting the maps for the 75th percentile PET, shown in Figure 8g–h.

3.4.2 | Trends

Figure 9 presents the 30-year long-term trends of hot bioclimate extremes, derived from the WRF simulations. A quick look reveals a predominant warming trend for all indices. Based on the analysis of the numerical simulations, the number of hot days (PET35) in the Euro-Mediterranean region has overall increased over the course of the examined 30-year period (Figure 9a). Statistically significant increasing trends of up to 1.5 days year^{-1} are mostly found in the eastern part of the domain, as well as in lowland areas in the central and west European Mediterranean. The number of very hot days (PET41) also shows increasing trends, but of lower magnitude (~0.5 days year^{-1}) and with spatially restricted statistical significance (Figure 9b).

Focusing on PETx, results suggest warming of the hottest days and nights in the study area. In terms of magnitude, positive trends are found to be larger for daytime (Figure 9d), approaching 0.3 °C year^{-1}, than for night-time (Figure 9c). The statistical significance of the computed trends appears not to have any particular spatial preference, although it can be seen that the northern latitudes of the domain show more widespread and coherent regions with statistically significant increasing trends. It is also worth noticing the presence of negative trends, which are most evident for the western part of the domain. In general, these trends are non-significant, except from over the IP, for parts of which statistically significant decreasing trends of up to −0.2 °C year^{-1} can be found in the case of daytime PETx (Figure 9d).

Larger trends are also found for the daytime than for the night-time 95th and 75th percentile PETs, as shown in Figure 9e–h. The computed trends reach up to 0.3 °C year^{-1} during the day and approximately 0.1 °C year^{-1} during the night for both PETp95 and PETp75. However, the most interesting feature of the presented maps is the presence of statistically significant increasing trends across the entire Euro-Mediterranean region, which provides solid evidence for warming of the hot tail of the distribution of PET. In particular, during the night (Figure 9e,g), both indices show nearly uniform statistically significant positive trends over the largest part of the domain, with non-significant trends confined to the western parts (FR, IP). In the daytime (Figure 9f,h), the positive trends retain in large the spatially extended statistical significance, especially over the north-eastern part of the study area (Balkan Peninsula, Turkey).

TABLE 3 The 1987–2016 trend per decade of cold PET-based extremes indices. For PET8 and PET4, units are days. For PETn, PETp5 and PETp25, units are °C

Region	PET8 0000 UTC	PET4 0000 UTC	PETn 0000 UTC	PETn 1200 UTC	PETp5 0000 UTC	PETp5 1200 UTC	PETp25 0000 UTC	PETp25 1200 UTC
IP	−2.52*	−1.41	−0.37*	−0.05	−0.06	−0.21**	−0.11	−0.16
FR	−1.34	−1.12	0.36	−0.17	0.07	0.07	−0.07	−0.04
AL	−2.95***	−4.25***	0.00	0.34	0.26	0.12	−0.03	−0.06
CMD	−3.61***	−4.55***	0.02	0.17	0.22	0.06	0.24**	0.02
BL	−7.72***	−6.04***	−0.40	−0.10	0.46	0.26	0.62**	0.46
SMD	−6.77***	−6.71***	0.02	−0.07	0.59	0.43	0.52***	0.64**

Note. AL = Alps; BL = Balkans; CMD = Central Mediterranean; FR = France; IP = Iberian Peninsula; SMD = south–east Mediterranean.

*Statistical significance at the 90% confidence interval ($.05 < p \leq .10$). **Statistical significance at the 95% confidence interval ($.01 < p \leq .05$). ***Statistical significance at the 99% confidence interval ($p \leq .01$).

Similarly to Table 3, Table 4 summarizes the computed trends per decade with different levels of statistical significance for hot bioclimate extremes indices. Overall, the results indicate warming of the hot facet of the thermal bioclimate. Almost all reported trends are positive, with most of them exhibiting the highest level of statistical significance. Over the course of the 1987–2016 period, hot (PET35) and very hot (PET41) days have been becoming more frequent, with the largest statistically significant ($p \leq .01$) trends, reaching up to 5 days per decade, found in the eastern part of the European Mediterranean (BL, SMD). The mean annual monthly maximum PET (PETx) also shows increasing trends in all regions, except from the IP for which non-significant decreasing trends are reported. Daytime trends for PETx are found to be larger than their night-time counterparts, reaching values of up to 0.60 °C per decade. Considering the hot tail of PET's distribution, the computed trends for PETp95 and PETp75 provide solid

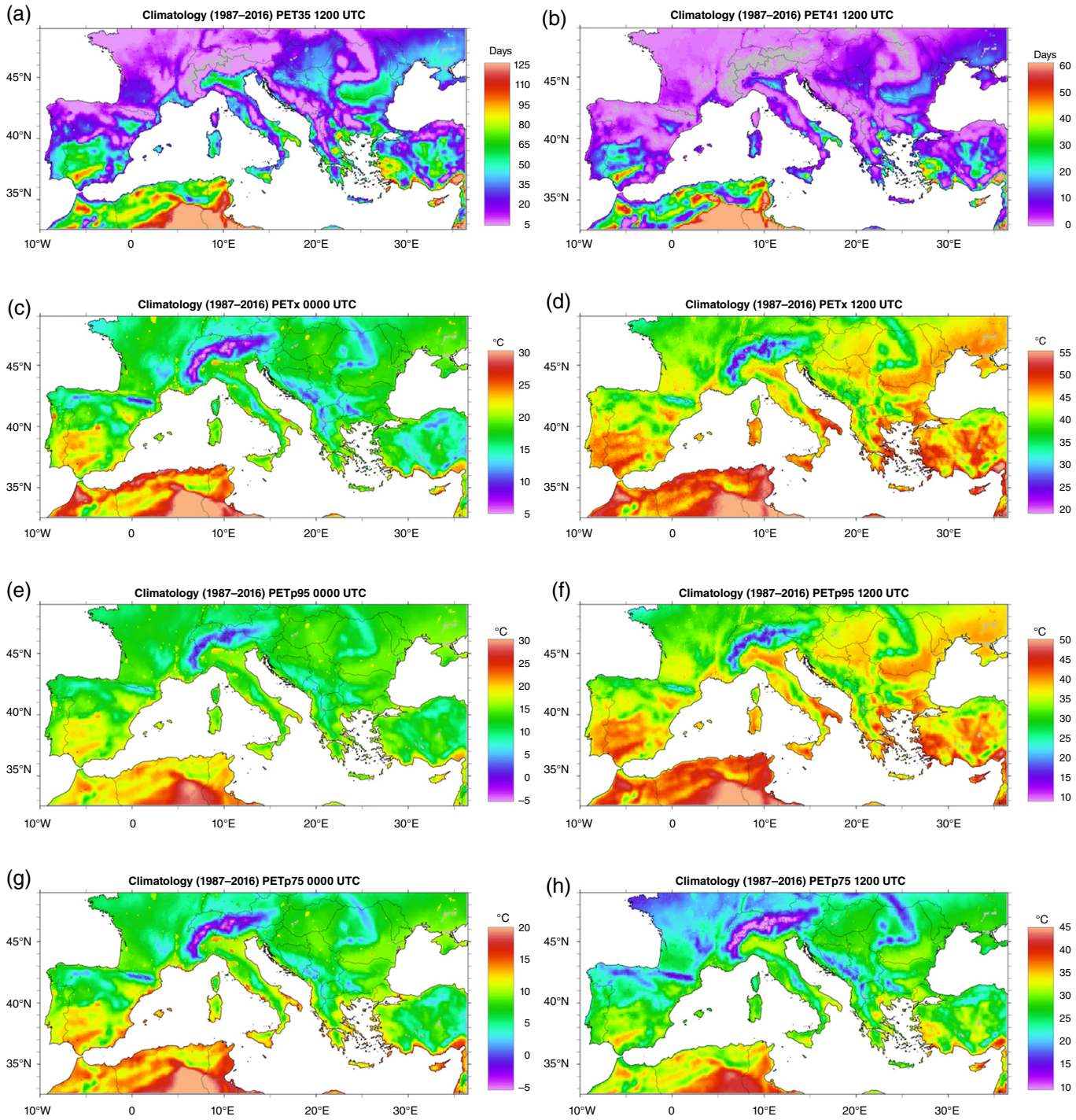

FIGURE 8 The 1987–2016 time mean of (a) PET35, (b) PET41, (c) 0000 UTC PETx, (d) 1200 UTC PETx, (e) 0000 UTC PETp95, (f) 1200 UTC PETp95, (g) 0000 UTC PETp75 and (h) 1200 UTC PETp75. Mind the differences in the scales [Colour figure can be viewed at wileyonlinelibrary.com]

evidence for statistically significant warming. In particular, it is worth highlighting the trends in the case of BL, which reach up to 0.9 and 1 °C per decade for the daytime 95th and 75th percentile PET, respectively.

4 | DISCUSSION

High-resolution numerical simulations, carried out with the WRF model, were employed for studying the climatology of the Euro-Mediterranean thermal bioclimate and for investigating the presence of long-term trends over the most recent 30-year period (i.e., 1987–2016), focusing on extremes. The numerical simulations were first evaluated against observational data for temperature, which is the key driver of variations in bioclimatic conditions (Basarin et al., 2017; Chen & Matzarakis, 2017; Giannaros et al., 2015). The evaluation procedure revealed an overall satisfactory model performance, characterized by mostly cold biases within the ranges reported in similar past modelling studies (Garciá-Diéz et al., 2013, 2015; Katragkou et al., 2015). The analysis of the thermal bioclimate was then carried out using 10 extremes-oriented indices, defined based on the RayMan-computed PET.

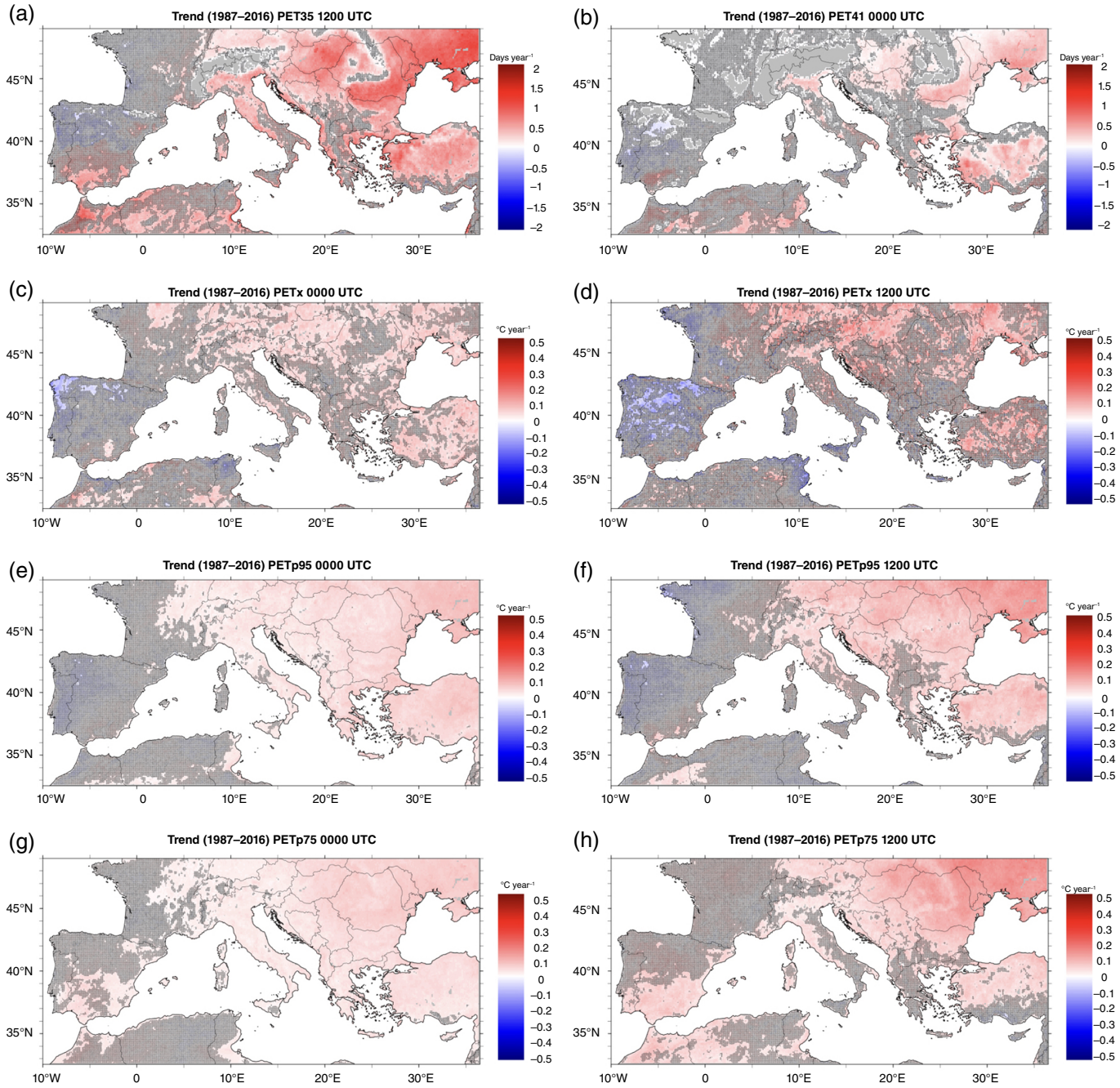

FIGURE 9 The 1987–2016 trend per year of (a) PET35, (b) PET41, (c) 0000 UTC PETx, (d) 1200 UTC PETx, (e) 0000 UTC PETp95, (f) 1200 UTC PETp95, (g) 0000 UTC PETp75 and (h) 1200 UTC PETp75. Hatching indicates grid points where the trends are not statistically significant, at least at the 90% confidence level ($p > .10$). Mind the differences in the scales [Colour figure can be viewed at wileyonlinelibrary.com]

The presented model-based climatology of the Euro-Mediterranean thermal bioclimate extremes agrees well with the results of similar past studies carried out on either a global (Jendritzky & Tinz, 2009; Matzarakis & Amelung, 2008) or a European scale (Matzarakis, Georgiadis, & Rossi, 2007; Tinz & Jendritzky, 2005). In particular, bioclimatic extremes exhibit a more or less zonal pattern, with heat (cold) stress occurring more frequently in the southern (northern) regions of the European Mediterranean. Topography acts on top of this spatial pattern, delineating areas of maxima and minima. It is worth noticing that these findings are in agreement with studies focusing on temperature and/or temperature-based extremes indices (e.g., Flaounas et al., 2013; Tanarhte, Hadjinicolaou, & Lelieveld, 2012; Xoplaki, González-Rouco, Luterbacher, & Wanner, 2003). Hence, they provide further evidence for the important role of temperature in shaping thermal bioclimate variations.

The time series analysis of the model-derived PET-based extremes indices suggests an overall warming trend that is generally larger in magnitude for cold bioclimate extremes. Results indicate that during the 1987–2016 period the decrease of cold days (PET < 8 °C) has been about twice as large as the increase of hot days (PET > 35 °C). This agrees with several studies reporting more rapid decrease of cold-related temperatures extremes than increase of warm/hot extremes (e.g., Alexander et al., 2006; Easterling et al., 1997; Stone & Weaver, 2002; Yan et al., 2002).

Considering the distribution of PET, the conducted analysis shows warming of both the cold and the warm tail. The highest 95th and 75th percentile PETs show statistically significant increasing trends that are larger during the day, whereas the lowest 5th and 25th percentiles show larger trend magnitudes in the night, with statistical significance verified only for the 25th percentile PET. In terms of spatial variability, the computed trends are most pronounced in the south–east European Mediterranean and the BL. This confirms previous studies that highlighted the above geographical regions of the Euro-Mediterranean region among the most responsive to warming (e.g., Efhtymiadis, Goodess, & Jones, 2011; Kostopoulou et al., 2014). On the other hand, wide parts of the Euro-Atlantic Mediterranean region (north–east IP, west FR) are found not to exhibit such warming trends and even show a cooling signal. This could indicate changes in the large-scale circulation patterns during the examined 30-year period. For instance, an increase in North Atlantic blocking situations could result to cooler temperatures, associated with the predominance of northerly advection. Another plausible explanation for the decreasing trends could be changes in cyclonic influence of these regions, which could affect warm air advection (e.g., Seubert et al., 2014).

5 | CONCLUSIONS

The results of this study provide evidence that the Euro-Mediterranean thermal bioclimate has undergone significant warming during the latest 30 years, which can be summarized in the decrease (increase) of cold (hot) extremes. As reported and discussed, the probability distribution of PET shows statistically significant warming considering both its cold and warm tail. This produces deteriorated, more stressful bioclimatic conditions that affect adversely human health and well-being. Furthermore, the shift towards a warmer thermal bioclimate is anticipated to influence energy demand and consumption for cooling, which in turn affects greenhouse gases' emissions (Matzarakis & Amelung, 2008).

The consideration of PET, which is a thermo-physiologically relevant index, broadens the usual practice of presenting maps focusing on a single parameter (e.g., temperature). Most importantly, the adopted approach allows for spatially assessing thermal stress, which is of paramount significance for human health and well-being. Within this context, problem-oriented information on the relationship between climate and climate change, and human health can be provided. Potential areas of future applications, related to the present work, include the sectors of tourism and recreation, energy and public health. For instance, the spatiotemporally detailed human biometeorological data could be employed for highlighting regions with favourable or less favourable thermal comfort conditions, which is an important aspect in tourism design applications. The reported trends' data could be also exploited for identifying areas that show high vulnerability to cold

TABLE 4 The 1987–2016 trend per decade of hot PET-based extremes indices. For PET35 and PET41, units are days. For PETx, PETp95 and PETp75, units are °C

Region	PET35 1200 UTC	PET41 1200 UTC	PETx 0000 UTC	PETx 1200 UTC	PETp95 0000 UTC	PETp95 1200 UTC	PETp75 0000 UTC	PETp75 1200 UTC
IP	1.05	0.18	−0.05	−0.31	−0.02	−0.01	0.21	0.39*
FR	0.41	0.05	0.20	0.01	0.14	−0.01	0.09	0.26
AL	1.46***	0.33***	0.35***	0.57**	0.31***	0.48***	0.27***	0.29**
CMD	2.55*	0.62	0.15	0.16	0.20**	0.24	0.23***	0.29*
BL	4.88***	1.24***	0.38*	0.60**	0.50***	0.88***	0.60***	0.98***
SMD	3.62***	2.00***	0.45**	0.44	0.57***	0.59***	0.43***	0.37**

*Statistical significance at the 90% confidence interval ($.05 < p \leq .10$). **Statistical significance at the 95% confidence interval ($.01 < p \leq .05$). ***Statistical significance at the 99% confidence interval ($p \leq .01$).

and hot stress, thus supporting policymaking related to public health, energy and tourism. Last but not least, it is the authors' strong belief that this work can be employed for increasing the awareness of the public with respect to the adverse impacts of the on-going climate change in the Euro-Mediterranean region.

ACKNOWLEDGEMENTS

The research leading to these results has been co-funded by the European Commission under the H2020 Research Infrastructures contract no. 675121 (project VI-SEEM). All numerical simulations have been produced using the GRNET's ARIS high-performance computing (HPC) infrastructure (https://hpc.grnet.gr/en/). We acknowledge the E-OBS dataset from the EU-FP6 project ENSEMBLES (http://ensembles-eu.metoffice. com) and the data providers in the ECA&D project (http://www. ecad.eu).

ORCID

Theodore M. Giannaros http://orcid.org/0000-0003-1138-3724

REFERENCES

Alexander, L. V., Zhang, X., Peterson, T. C., Caesar, J., Gleason, B., Klein-Tank, A. M. G., … Vasquez-Aguirre, J. L. (2006). Global observed changes in daily climate extremes of temperature and precipitation. *Journal of Geophysical Research*, *111*, D05109.

Amengual, A., Homar, V., Romero, R., Brooks, H. E., Ramis, C., Gordaliza, M., & Alonso, S. (2014). Projections of heat waves with high impact on human health in Europe. *Global Planeteray Change*, *119*, 71–84.

Basarin, B., Lukić, T., Mesaroš, M., Pavić, D., Dordević, J., & Matzarakis, A. (2017). Spatial and temporal analysis of extreme bioclimate conditions in Vojvodina, Northern Serbia. *International Journal of Climatology*, *38*, 142–157. https://doi.org/10.1002/joc.5166

Błażejczyk, K. (1994). New climatological-and-physiological model of the human heat balance outdoor (MENEX) and its applications in bioclimatological studies in different scales. In K. Błażejczyk & B. Krawczyk (Eds.), *Bioclimatic research of the human heat balance. Zeszyty IGiPZ PAN 28* (pp. 27–58). Warsaw, Poland: Polish Academy of Sciences.

Błażejczyk, K., Epstein, Y., Jendritzky, G., Staiger, H., & Tinz, B. (2011). Comparison of UTCI to selected thermal indices. *International Journal of Biometeorology*, *56*, 515–535.

BOHS. (1996). *The thermal environment. British Occupational Hygiene Society Technical Guide No. 12* (2nd ed.). Leeds, England: Scientific Consultants Ltd.

Bolle, H. J. (2002). *Mediterranean climate: Vulnerability and trends*. New York, NY: Springer.

Brosy, C., Zaninovic, K., & Matzarakis, A. (2014). Quantification of climate tourism potential of Croatia based on measured data and regional modeling. *International Journal of Biometeorology*, *58*, 1369–1381.

Brown, R. D., & Gillespie, T. J. (1986). Estimating outdoor thermal comfort using a cylindrical radiation thermometer and an energy budget model. *International Journal of Biometeorology*, *30*, 43–52.

Büttner, K. (1938). *Physikalische Bioklimatologie*. Leipzig, Germany: Akademische.

Carder, M., McNamee, R., Beverland, I., Elton, R., Cohen, G. R., Boyd, J., & Agius, R. M. (2005). The lagged effect of cold temperature and wind chill on cardiorespiratory mortality in Scotland. *Occupational and Environmental Medicine*, *62*, 702–710.

Charalampopoulos, I., Tsiros, I., Chronopoulou-Sereli, A., & Matzarakis, A. (2013). Analysis of thermal bioclimate in various urban configurations in Athens, Greece. *Urban Ecosystems*, *16*, 217–233.

Chen, Y.-C., & Matzarakis, A. (2017). Modified physiologically equivalent temperature—Basics and applications for western European climate. *Theoretical and Applied Climatology*, 1–15. https://doi.org/10.1007/s00704-017-2158-x

Daneshvar, M. R. M., Bagherzadeh, A., & Tavousi, T. (2013). Assessment of bioclimatic comfort conditions based on physiologically equivalent temperature (PET) using the RayMan model in Iran. *Central European Journal of Geosciences*, *5*, 53–60.

De Freitas, C. R., Matzarakis, A., & Scott, D. (2007). Climate, tourism and recreation: a debate of the ISB's Commission on climate, tourism and recreation. In *Proceedings of the 3rd International Workshop on Climate, Tourism and Recreation*, 19–22 September, 2007, Alexandroupolis, Greece.

Dee, D. P., Uppala, S. M., Simmons, A. J., Berrisfort, P., Poli, P., Kobayashi, S, … Vitard, F. (2011). The ERA-Interim reanalysis: Configuration and performance of the data assimilation system. *Quarterly Journal of the Royal Meteorological Society*, *137*, 553–597.

Diffenbaugh, N. S., Pal, J. S., Giorgi, F., & Gao, X. (2007). Heat stress intensification in the Mediterranean climate change hotspot. *Geophysical Research Letters*, *34*, L11706.

Easterling, D. R., Horton, B., Jones, P. D., Peterson, T. C., Karl, T. R., Parker, D. E., … Folland, C. K. (1997). Maximum and minimum temperatures for the globe. *Science*, *277*, 364–367.

Efhtymiadis, D., Goodess, C. M., & Jones, P. D. (2011). Trends in Mediterranean gridded temperature extremes and large-scale circulation influences. *Natural Hazards and Earth System Sciences*, *11*, 2199–2214.

Endler, C., & Matzarakis, A. (2011). Climatic potential for tourism in the Black Forest, Germany—Winter season. *International Journal of Biometeorology*, *55*, 339–351.

Fanger, P. O. (1970). *Thermal comfort: Analysis and applications in environmental engineering*. New York, NY: McGraw-Hill.

Fanger, P. O. (1972). *Thermal comfort*. New York, NY: McGraw-Hill.

Flaounas, E., Drobinski, P., Vrac, M., Bastin, M., Lebeaupin-Brossier, C., Stéfanon, M., … Calvet, J.-C. (2013). Precipitation and temperature space-time variability and extremes in the Mediterranean region: Evaluation of dynamical and statistical downscaling methods. *Climate Dynamics*, *40*, 2687–2705.

Garciá-Diéz, M., Fernández, J., Fita, L., & Yagüe, C. (2013). Seasonal dependence of WRF model biases and sensitivity to PBL schemes over Europe. *Quarterly Journal of the Royal Meteorological Society*, *139*, 501–514.

Garciá-Diéz, M., Fernández, J., & Vautard, R. (2015). An RCM multi-physics ensemble over Europe: Multi-variable evaluation to avoid error compensation. *Climate Dynamics*, *45*, 3141–3156.

Giannaros, T. M., & Melas, D. (2012). Study of the urban heat island in a coastal Mediterranean city: The case study of Thessaloniki, Greece. *Atmospheric Research*, *118*, 103–120.

Giannaros, T. M., Melas, D., & Matzarakis, A. (2015). Evaluation of thermal bioclimate based on observational data and numerical simulations: An application to Greece. *International Journal of Biometeorology*, *59*, 151–164.

Giorgi, F. (2006). Climate change hot-spots. *Geophysical Research Letters*, *33*, L08707.

Gosling, S. N., Lowe, J. A., McGregor, G. R., Pelling, M., & Malamud, B. D. (2009). Associations between elevated atmospheric temperature and human mortality: A critical review of the literature. *Climatic Change*, *92*, 299–341.

Grell, G., & Devenyi, D. (2002). A generalized approach to parameterizing convection combining ensemble and data assimilation techniques. *Geophysical Research Letters*, *29*, L01693.

Haylock, M. R., Hofstra, N., Klein Tank, A. M. G., Klok, E. J., Jones, P. D., & New, M. (2008). A European daily high-resolution gridded data set of surface temperature and precipitation for 1950-2006. *Journal of Geophysical Research*, *113*, D20119.

Herrera, S., Fita, L., Fernández, J., & Gutiérrez, J. (2010). Evaluation of the mean and extreme precipitation regimes from the ENSEMBLES regional climate multimodel simulations over Spain. *Journal of Geophysical Research*, *115*, D21117.

Hofstra, N., Haylock, M., New, M., & Jones, P. D. (2009). Testing E-OBS European high-resolution gridded dataset of daily precipitation and surface temperature. *Journal of Geophysical Research*, *114*, D011799.

Holmer, I. (2011). Chapter 42: Cold indices and standards. In *ILO encyclopedia of occupational health and safety* (Vol. *2*). Geneva: International Labor Organization. Retrieved from http://www.iloencyclopaedia.org/part-vi-16255/heat-and-cold/42/cold-indices-and-standards

Hong, S. Y., Noh, Y., & Dudhia, J. (2006). A new vertical diffusion package with an explicit treatment of entrainment processes. *Monthly Weather Review*, *134*, 2318–2341.

Höppe, P. (1993). Heat balance modeling. *Experientia*, *49*, 741–746.

Höppe, P. (1999). The physiological equivalent temperature—A universal index for the biometeorological assessment of the thermal environment. *International Journal of Biometeorology*, *43*, 71–75.

Iacono, M. J., Delamere, J. S., Mlawer, E. J., Shephard, M. W., Clough, S. A., & Collins, W. D. (2008). Radiative forcing by long-lived greenhouse gases: Calculations with the AER radiative transfer models. *Journal of Geophysical Research*, *113*, D13103.

ISO7730. (2005). *ISO7730: Ergonomics of the thermal environment: Analytical determination and interpretation of thermal comfort using calculation of the PMV and PDD indices and local thermal comfort criteria*. Geneva, Switzerland: ISO.

Jendritzky, G. (1991). Selected questions of topical interest in human bioclimatology. *International Journal of Biometeorology*, *35*, 139–150.

Jendritzky, G., & Nübler, W. (1981). A model analyzing the urban thermal environment in physiologically significant terms. *Archives for Meteorology, Geophysics, and Bioclimatology Series B*, *29*, 313–326.

Jendritzky, G., & Tinz, B. (2009). The thermal environment of the human being on a global scale. *Global Health Action*, *2*, 1–18.

Junk, J., Matzarakis, A., Ferrone, A., & Krein, A. (2014). Evidence of past and future changes in health-related meteorological variables across Luxemburg. *Air Quality, Atmosphere and Health*, *7*, 71–81.

Katragkou, E., Garciá-Diéz, M., Vautard, R., Sobolowski, S., Zanis, P., Alexandri, G., … Jacob, D. (2015). Regional climate hindcast simulations within EURO-CORDEX: Evaluation of a WRF multi-physics ensemble. *Geoscientific Model Development*, *8*, 603–618.

Kendall, M. G. (1976). *Rank correlation methods* (4th ed.). London, England: Griffin.

Kerslake, D. M. K. (1972). *The stress of hot environments*. Cambridge, England: Cambridge United Press.

Kioutsioukis, I., de Meij, A., Jakobs, H., Katragkou, E., Vinuesa, J.-F., & Kazantzidis, A. (2016). High resolution WRF ensemble forecasting for irrigation: Multi-variable evaluation. *Atmospheric Research*, *167*, 156–174.

Kosatsky, T. (2005). The 2003 European heat waves. *Euro Surveillance*, *10*, 148–149.

Kostopoulou, E., Giannakopoulos, C., Hatzaki, M., Karali, A., Hadjinicolaou, P., Lelieveld, J., & Lange, M. A. (2014). Spatio-temporal patterns of recent and future climate extremes the eastern Mediterranean and Middle East region. *Natural Hazards and Earth System Sciences*, *14*, 1565–1577.

Kotlarski, S., Keuler, K., Christensen, O. B., Colette, A., Déqué, M., Gobiet, A., … Wulfmeyer, V. (2014). Regional climate modeling on European scales: A joint standard evaluation of the EURO-CORDEX RCM ensemble. *Geoscientific Model Development*, *7*, 1297–1333.

Kovats, S. R., & Jendritzky, G. (2006). Heat-waves and human health. In B. Menne & K. L. Ebi (Eds.), *Climate change and adaptation strategies for human health* (pp. 63–97). Darmstadt, Germany: Steinkopff.

Kysely, J., & Plavcova, E. (2010). A critical remark on the applicability of E-OBS European gridded temperature dataset for validating control climate simulations. *Journal of Geophysical Research*, *115*, D014123.

Laschewski, G., & Jendritzky, G. (2002). *Effects of the thermal environment on human health: And investigation of 30 years of daily mortality data from SW Germany*. Deutscher Wetterdienst, Germany: Business Unit Human Biometeorology.

Lin, T. P., & Matzarakis, A. (2011). Tourism-climate information based on human thermal perception in Eastern China and Taiwan. *Tourism Management*, *32*, 492–500.

Lin, Y. L., Farley, R. D., & Orville, H. D. (1983). Bulk parameterization of the snow field in a cloud model. *Journal of Climate and Applied Meteorology*, *22*, 1065–1092.

Lionello, P., Malanotte-Rizzoli, P., Boscolo, R., Alpert, P., Artale, V., Li, L., … Xoplaki, E. (2006). The Mediterranean climate: An overview of the main characteristics and issues. In P. Lionello, P. Malanotte-Rizzoli, & R. Boscolo (Eds.), *Mediterranean climate variability* (pp. 1–26). Amsterdam, the Netherlands: Elsevier.

Mann, H. B. (1945). Nonparametric tests against trend. *Econometrica*, *13*, 245–259.

Matzarakis, A. (2007). Assessment method for climate and tourism based on daily data. In A. Matzarakis, C. R. de Freitas, & D. Scott (Eds.), *Developments in tourism climatology* (pp. 52–58). Freiburg, Germany: International Socieity of Biometeorology.

Matzarakis, A., & Amelung, B. (2008). Physiologically equivalent temperature as indicator for impacts of climate change on thermal comfort of humans. In M. C. Thomson, R. Garcia-Herrera, & M. Beniston (Eds.), *Seasonal forecasts, climatic change and human health* (pp. 161–172). Netherlands: Springer Netherlands.

Matzarakis, A., Georgiadis, T., & Rossi, F. (2007). Thermal bioclimate analysis for Europe and Italy. *Il Nuovo Cimento*, *30*, 623–631. https://doi.org/10.1393/ncc/i2007-10268-0

Matzarakis, A., & Mayer, H. (1997). Heat stress in Greece. *International Journal of Biometeorology*, *41*, 34–39.

Matzarakis, A., Mayer, H., & Iziomon, M. G. (1999). Applications of a universal thermal index: Physiological equivalent temperature. *International Journal of Biometeorology*, *43*, 76–84.

Matzarakis, A., Muthers, S., & Koch, E. (2011). Human biometeorological evaluation of heat-related mortality in Vienna. *Theoretical and Applied Climatology*, *105*, 1–10.

Matzarakis, A., Rutz, F., & Mayer, H. (2007). Modeling radiation fluxes in simple and complex environments—Application of the RayMan model. *International Journal of Biometeorology*, *51*, 323–334.

Matzarakis, A., Rutz, F., & Mayer, H. (2010). Modeling radiation fluxes in simple and complex environments: Basics of the RayMan model. *International Journal of Biometeorology*, *54*, 131–139.

McGregor, G. R. (2011). Human biometeorology. *Progress in Physical Geography*, *36*, 93–109.

Morillón-Gálvez, D., Saldana-Flores, R., & Tejeda-Martinez, A. (2004). Human bioclimatic atlas for Mexico. *Solar Energy*, *76*, 781–792.

Muthers, S., Laschewski, G., & Matzarakis, A. (2017). The summers 2003 and 2015 in south-West Germany: Heat waves and heat-related mortality in the context of climate change. *Atmosphere*, *8*, 224. https://doi.org/10.3390/atmos8110224

Muthers, S., Matzarakis, A., & Koch, E. (2010). Climate change and mortality in Vienna—A human biometeorological analysis based on regional climate modeling. *International Journal of Environmental Research and Public Health*, *7*, 2965–2977.

Nastos, P. T., & Matzarakis, A. (2006). Weather impacts on respiratory infections in Athens, Greece. *International Journal of Biometeorology*, *50*, 358–369.

Orosa, J. A., Costa, A. M., Rodríguez-Fernández, A., & Roshan, G. (2014). Effect of climate change on outdoor thermal comfort in humid climates. *Journal of Environmental Health Science and Engineering*, *12*, 46.

Parsons, K. C. (2011). Chapter 42: Assessment of heat stress and heat stress indices. In *ILO Encyclopedia of occupational health and safety* (Vol. *2*). Retrieved from http://www.iloencyclopaedia.org/part-vi-16255/heat-and-cold/42/assessment-of-heat-stress-and-heat-stress-indicies

Parsons, K. C. (2003). *Human thermal environments: The effects of hot, moderated and cold environments on human health, comfort and performance*. New York, NY: Taylor and Francis.

Poupkou, A., Nastos, P., Melas, D., & Zerefos, C. (2011). Climatology of discomfort index and air quality index in a large urban Mediterranean agglomeration. *Water, Air and Soil Pollution*, *222*, 163–183.

Robine, J.-M., Cheung, S. L. K., Le Roy, S., Van Oyen, H., Griffiths, C., Michel, J.-P., & Herrmann, F. R. (2008). Death toll exceeded 70,000 in Europe during the summer of 2003. *Comptes Rendus Biologies*, *331*, 171–178.

Schär, C., & Jendritzky, G. (2004). Climate change: Hot news from summer 2003. *Nature*, *432*, 559–560.

Segnalini, M., Nardone, A., & Bernabucci, U. (2011). Dynamics of the temperature-humidity index in the Mediterranean basin. *International Journal of Biometeorology*, *55*, 253–263.

Seubert, S., Fernández-Montes, S., Philipp, A., Herting, E., Jacobeit, J., Vogt, G., … Paeth, H. (2014). Mediterranean climate extremes in synoptic downscaling assessments. *Theoretical and Applied Climatology*, *117*, 275–275.

Sibbons, J. L. (1966). Assessment of thermal stress from energy balance considerations. *Journal of Applied Physiology*, *21*, 1207–1217.

Skamarock, W. C., Klemp, J. B., Dudhia, J., Gill, D. O., Barker, D. M., Duda, M. G., . . . Powers, J. G. (2008). *A description of the Advanced*

Research WRF version 3. NCAR Technical Note, NCAR/TN-475+STR, June 2008, Boulder, CO, 125 pp.

Stone, D. A., & Weaver, A. J. (2002). Daily maximum and minimum temperature trends in a climate model. *Geophysical Research Letters*, *29*, L01356.

Svensson, M., Thorsson, S., & Lindqvist, S. (2003). A GIS model for creating bioclimatic maps—Examples from a high mid-latitude city. *International Journal of Biometeorology*, *47*, 102–112.

Tanarhte, M., Hadjinicolaou, P., & Lelieveld, J. (2012). Intercomparison of temperature and precipitation datasets based on observations in the Mediterranean and the Middle East. *Journal of Geophysical Research*, *117*, D12102.

Tewari, M., Chen, F., Wang, W., Dudhia, J., LeMone, M. A., Mitchell, K., . . . Cuenca, R. H. (2004). Implementation and verification of the unified NOAH land surface model in the WRF model. Paper presented at the 20th Conference on Weather Analysis and Forecasting/16th Conference on Numerical Weather Prediction, 10–15 January 2004, Seattle, WA.

Tinz, B., & Jendritzky, G. (2005). Macro- and mesoscale maps of the thermal environment. In 17th International Congress of Biometeorology. *Annals of Meteorology*, *41*, 641–643.

Topay, M. (2013). Mapping of thermal comfort for outdoor recreation planning using GIS: The case of Isparta Province (Turkey). *Turkish Journal of Agriculture and Forestry*, *37*, 110–120.

United Nations World Tourism Organization. (2009). *World tourism barometer*. Madrid, Spain: United Nations.

Vanos, J. K., Warland, J. S., Gillespie, T. J., & Kenny, N. A. (2010). Review of the physiology of human thermal comfort while exercising in urban landscapes and implications for bioclimatic design. *International Journal of Biometeorology*, *54*, 319–334.

Xoplaki, E., González-Rouco, J. F., Luterbacher, J., & Wanner, H. (2003). Mediterranean summer air temperature variability and its connection to the large-scale atmospheric circulation and SSTs. *Climate Dynamics*, *20*, 723–739.

Yan, Z., Jones, P. D., Moberg, A., Bergström, H., Camuffo, D., Cocheo, C., … Yang, C. (2002). Trends of extreme temperatures in Europe and China based on daily observations. *Climatic Change*, *53*, 355–392.

Yao, R., Li, B., & Liu, J. (2009). A theoretical adaptive model of thermal comfort: Adaptive predicted mean vote (aPMV). *Building and Environment*, *44*, 2089–2096.

Yue, S., Pilon, P., Phinney, B., & Cavadias, G. (2002). The influence of autocorrelation on the ability to detect trends in hydrological series. *Hyrdological Processes*, *16*, 1807–1829.

Zaninovic, K., & Matzarakis, A. (2009). The bioclimatological leaflet as a means conveying climatological information to tourists and the tourism industry. *International Journal of Biometeorology*, *53*, 369–374.

Zhang, D. L., & Anthes, R. A. (1982). A high-resolution model of the planetary boundary layer—Sensitivity tests and comparison with SESAME-79 data. *Journal of Applied Meteorology*, *21*, 1594–1609.

Zygmuntowski, M., Matzarakis, A., Koch, E., & Rudel, E. (2005). Comparison of climate and SYNOP measurements for the bioclimate of Austria. *Annalen der Meteorologie*, *41*, 644–647.

How to cite this article: Giannaros TM, Kotroni V, Lagouvardos K, Matzarakis A. Climatology and trends of the Euro-Mediterranean thermal bioclimate. *Int J Climatol*. 2018;1–19. https://doi.org/10.1002/joc.5501